FISEVIER

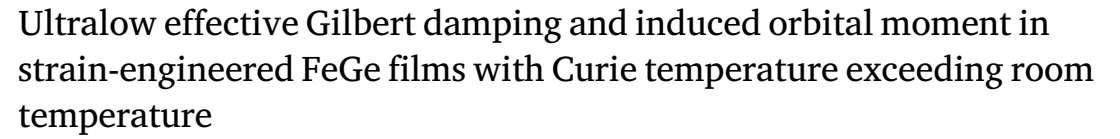
Contents lists available at ScienceDirect

Journal of Magnetism and Magnetic Materials

journal homepage: www.elsevier.com/locate/jmmm



Research article



Sujan Budhathoki ^a, Arjun Sapkota ^a, Ka Ming Law ^a, Smriti Ranjit ^a, Gregory M. Stephen ^b, Don Heiman ^{b,c}, Michelle E. Jamer ^d, Tim Mewes ^a, Adam J. Hauser ^{a,*}

- ^a Department of Physics and Astronomy, The University of Alabama, Tuscaloosa AL 35487, USA
- ^b Physics Department, Northeastern University, Boston, MA 02115, USA
- c Plasma Science and Fusion Center, MIT, Cambridge, MA 02139, USA
- ^d Physics Department, United States Naval Academy, Annapolis, MD 21402, USA

ARTICLE INFO

Keywords: Gilbert damping Spin damping FeGe Thin films X-ray magnetic circular dichroism (XMCD) Ferromagnetic resonance

ABSTRACT

We report the magnetic and magnetodynamic properties of strained epitaxial FeGe thin films on Ge(111) substrates, and confirm the generation of orbital moment in tensile-strained FeGe not seen in bulk or unstrained films. In-plane tensile strain resulted in an increase of the magnetic transition temperature to 350 K, likely the result of decreased Fe–Fe bond lengths that increase spin–orbit coupling strength. X-ray magnetic circular dichroism (XMCD) shows orbital-to-spin magnetic moment ratios of 0.18 and 0.14 for films of 18 nm and 72 nm thickness, respectively, indicative of partially quenched atomic orbitals. A very low effective Gilbert damping parameter, $\alpha_{eff} = 0.003 \pm 0.001$ at room temperature was observed, suggesting that strained FeGe could be useful for spintronic applications.

Noncollinear magnetism presents a rich magnetic phase diagram exhibiting various ground state spin modulations such as helical, conical, spin spiral or non-trivial topological magnetic skyrmions. These topological entities have been viewed as potential solutions for energy efficient, non-volatile memory storage applications due to ultra-low current density requirements for domain wall manipulation [1–5]. Skyrmions emerge in systems that exhibit Dzyaloshinskii–Moriya interaction (DMI) caused by inversion symmetry breaking [6,7] at the thin film interfaces or in bulk crystal [8–12] of noncentrosymmetric cubic helimagnets such as FeGe [1,13], MnSi [14] or FeCoSi [15]. Among reported B20 compounds, FeGe has the highest bulk ordering temperature $T_c \sim 278$ K [1–3] making it a promising candidate for future spintronic device applications.

Realization of skyrmion-based spintronic memory devices requires a ferromagnetic material with Curie temperature (T_c) above room temperature, as the skyrmion crystal lattice (SkX) phase in B20 compounds is typically realized just below T_c [14,16,17]. Previous work has shown a strong topological Hall effect between 10 K and 330 K for strained FeGe films, with strong increase in signal at 330 K consistent with a potential SkX phase [18]. Epitaxial strain has been shown to lead to substantial increase in T_c [19,20]. Our previous work on strained FeGe films grown on Ge substrate has shown a class-best T_c = 350 K [18]

among B20 compounds. However, epitaxial strain can also result in higher structural disorder and grain boundary density.

Epitaxial FeGe(111) thin films with thicknesses 18 nm and 72 nm were grown on Ge(111) substrates using our custom built off-axis sputter beam epitaxy (SBE) [21,22] system (AJA International Inc) by co-sputtering of elemental Fe and Ge targets, and were capped with Al (2.7 nm). Details of the growth and film quality, and partial characterization of the 18 nm film studied further below were published previously [18]. In that paper, it was hypothesized that the system underwent a strain-mediated rhombohedral distortion that resulted in a significant increase in the magnetic ordering temperature compared to bulk [18].

In this work, we examine the magnetic structure of the strained FeGe thin film system in greater detail. The 18 nm and 72 nm films in this study were previously found to have identical compositions as well as identical lattice constants consistent with 4.1% epitaxial tensile strain [18], with no evidence of strain relaxation in either film. Through magnetometry, we confirm the same Curie temperature $T_c=350~{\rm K}$ for the 72 nm film as for the 18 nm film, and saturation magnetization exceeding the 1 $\mu_B/{\rm f.u.}$ spin-moment-only value observed in bulk and

E-mail address: ahauser@ua.edu (A.J. Hauser).

^{*} Corresponding author.

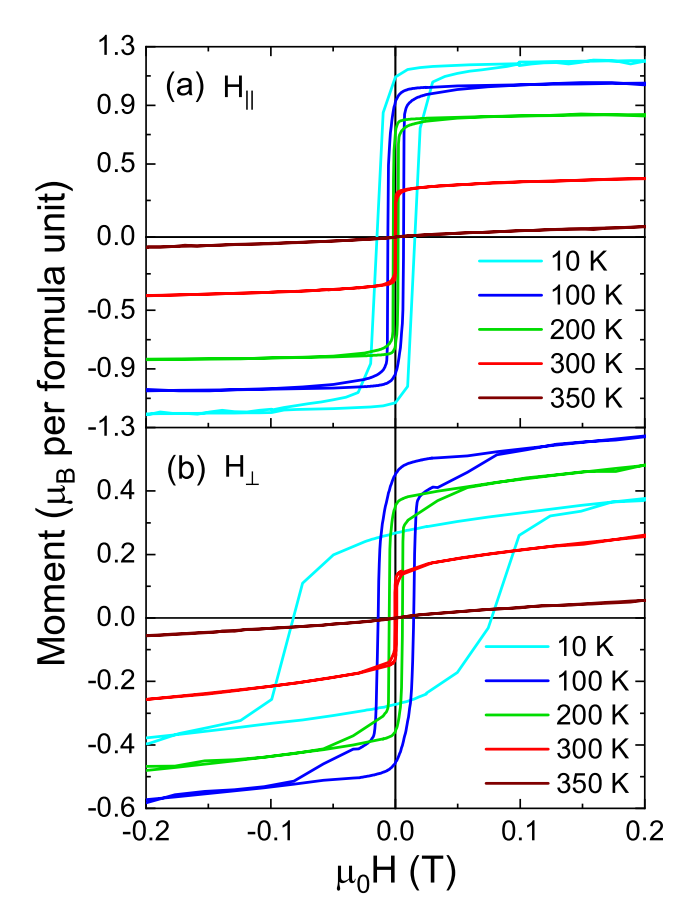


Fig. 1. Magnetic hysteresis loops at different temperatures for 72 nm thick FeGe film measured by SQUID magnetometry for both (a) in-plane (field parallel to film plane) and (b) out-of-plane (field perpendicular to film plane) configuration.

unstrained thin films. X-ray magnetic circular dichroism (XMCD) measurements show the emergence of significant orbital moment in both the 18 nm and 72 nm films, with semi-quantitative m_l/m_s ratios (0.18 and 0.14, respectively) that roughly fit the increase in total magnetic moments observed in the films. Finally, we investigate the dynamic properties of the 72 nm film by ferromagnetic resonance (FMR) measurements, finding Gilbert damping parameters 2–3 times lower than reported previously for the 18 nm films and g-values corroborating the significant orbital moment found by XMCD.

Magnetic properties were investigated by two systems: a Quantum Design superconducting quantum interference device (SQUID), and a vibrating sample magnetometer (VSM) option for the physical property measurement system (PPMS, also by Quantum Design). Fig. 1 shows the magnetic hysteresis behavior for both in-plane (IP) and out-ofplane (OP) geometry, and from 10 K to 350 K, for the 72 nm film. The saturation magnetization was determined to be $M_s = 1.24(2)$ and 1.15(6) $\mu_R/\text{f.u.}$ for the 72 nm and 18 nm thick films at 10 K, respectively. This observed saturation magnetization is larger than the bulk value of 1 μ_B /f.u. for the bulk FeGe [23,24]. We show later in this paper that the additional moment is likely orbital in nature, ascribed to strain-generated spin-orbit coupling. We observed a larger coercivity (H_c) at 10 K, both the magnitude and increase at low temperature is fairly typical for OP axis for a coherent ferromagnetic thin film [25,26]. We also observed a strong remanence at lower temperatures. There is some possibility one could investigate the resultant perpendicular magnetic anisotropy (PMA) [25,26] but would likely require a more robust series of thicknesses for conclusive results.

The Curie temperature was determined from isothermal magnetization measurements, through the Arrott plot [27] method (in mean

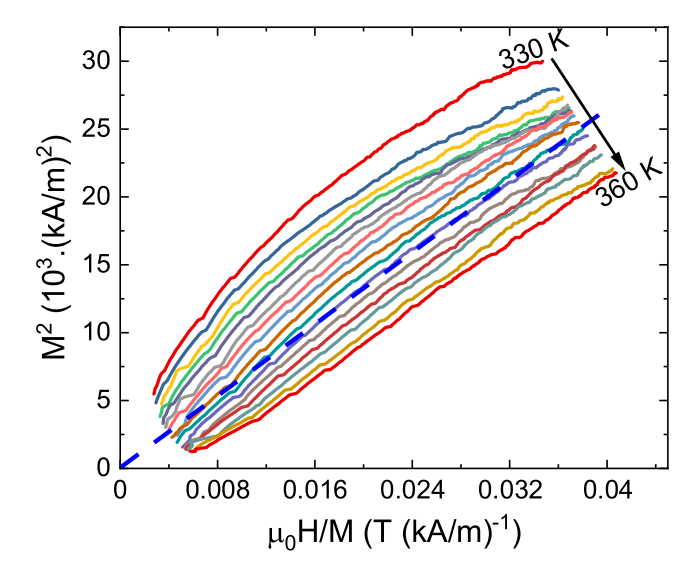


Fig. 2. Arrott plot (M^2 Vs. H/M) of magnetization isotherms for 72 nm thick FeGe film measured by VSM. Isotherms are spaced 2 K apart. The Blue dashed line indicates the isotherm extrapolation to the origin indicating Curie temperature of 350 K.

field approximation). Fig. 2 shows magnetic isotherms with 2 K step size from 330 K to 360 K, i.e. the Arrott curves (plot of M^2 vs. H/M). The T_c was then estimated by the isotherm at 350 K that extrapolates to zero (see Supplementary material for additional information [28]). Above 350 K, the curves show a paramagnetic behavior dictated by the linear curves, whereas the Arrott curves are not linear below 350 K. The enhancement of T_c over the bulk value of 278 K [1–3] and magnetic moment is attributed to the modulation in the spin–spin coupling caused by the substrate-induced in-plane tensile strain in FeGe thin films inducing a rhombohedral distortion [18]. This modifies the interplanar spacing between FeGe(111) planes, thereby decreasing the Fe–Fe bond length which consequently causes enhancement of the ordering temperature [18].

Element-specific X-ray absorption spectroscopy (XAS) and X-ray magnetic circular dichroism (XMCD) measurements were performed at Beamline 4.0.2 of the Advanced Light Source at Lawrence Berkeley National Laboratory using circularly polarized X-rays with ~90% spin polarization. X-ray absorption (XA) spectra at the Fe $L_{3,2}$ -edges were probed in both total electron yield mode (TEY) and fluorescence yield (FY) mode with the X-ray beam at an angle of 30° from the plane of the film surface and magnetic field applied parallel to the beam. XMCD probes the element specific magnetic moment by aligning a magnetic field both parallel and anti-parallel to the photon helicity, and subtracting the two spectra. This difference is the dichroism signal, and by comparing the areas underneath the L_3 and L_2 peaks, the spin-to-orbit ratio can be estimated from "sum rule" calculations [29–31].

XA and XMCD spectra for the 18 nm and 72 nm thick films probed in TEY mode are illustrated in Fig. 3(a) and (b). (See Supplementary material for spectra probed in FY mode [28]). The penetration depth of X-rays at the Fe L-edge energy range makes this measurement a probe of the top 10 nm of each film. At 300 K and at \pm 400 mT applied magnetic field, the XA spectra at the Fe *L*-edges correspond well to metallic Fe reference spectra [32,33].

The values extracted for the respective areas (for XA spectra probed in TEY mode) are listed in Table 1, and the equations to calculate the magnetic orbital moment (m_l) and spin moment (m_s) are as follows [29–31]:

$$m_l = -\frac{4}{3} n_\hbar \mu_B \frac{A+B}{C},\tag{1}$$

$$m_s = -n_h \mu_B \frac{2A - 4B}{C},\tag{2}$$

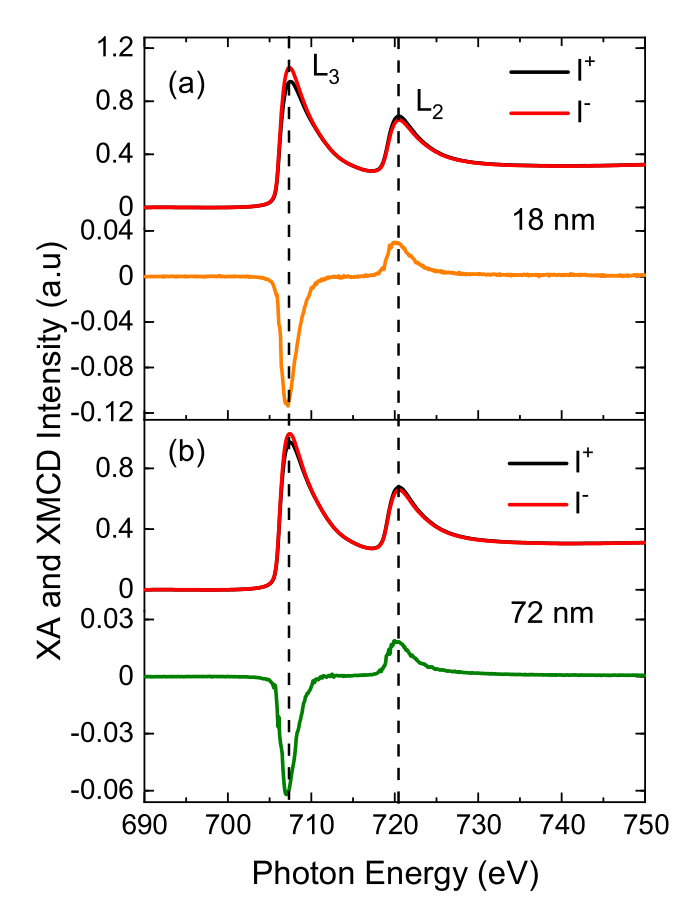


Fig. 3. XA and XMCD spectra for Fe $L_{3,2}$ edges for (a) 18 nm and (b) 72 nm thick FeGe film probed in TEY mode at 300 K.

where n_h is the number of holes in the d-valence shell, C is the total area under the normalized XA curve, A is the area under the L_3 dichroism curve, and B is the area under the L_2 dichroism curve. In both samples, the spin moment is larger than the orbital moment, indicative of the partially quenched orbital moment, typical of 3d transition elements. The L_3 dichroism in the 72 nm thick film is significantly larger, both in magnitude and proportionality to previous XMCD results on bulk FeGe, suggesting that our films are not fully analogous to a bulk state, even at 72 nm thickness [34].

Calculating the magnetic moment of various 3d transition metal elements through XMCD and the sum rule has a variable amount of inherent (intrinsic errors that limit the application of the XMCD spin sum rule, including difficulty in accurately determining n_h for each film) errors based on the d-orbital occupations, as well as systematic errors (including background subtraction and curve integration). For instance, looking at the two dichroism curves in Fig. 3(a) and (b), the area under the curve for the 72 nm sample is smaller than the 18 nm, but the difference magnitudes are small compared to the XA spectra and small changes in background subtraction choices (as well as error in n_h) could produce variations on the order of the difference of the dichroism spectra.

As an alternative, we take a semi-quantitative approach to our goal of understanding the source of strained FeGe's enhanced magnetic properties. XMCD spectra probed in TEY mode were analyzed to extract the spin-to-orbit ratios [29–31]. We compare the A and B values as shown in Table 1 and extract the ratio of the orbital moment (m_l) to the spin moment (m_s) , $\frac{m_l}{m_s} = \frac{2A+2B}{3A-6B}$, which gives a value of 0.14 for the 72 nm thick film and 0.18 for the 18 nm thick film. This ratio yields the evidence of significant orbital moment that we are seeking, with less influence from the sources of error stated above.

Table 1 The calculated areas A, B and C under the dichroism curve L_3 , L_2 and normalized XA curve respectively and m_l/m_s ; the ratio of orbital to spin

Sample	A	В	С	m_l/m_s
72 nm	-0.1448	0.0796	7.142	0.14
18 nm	-0.2754	0.1311	7.312	0.18

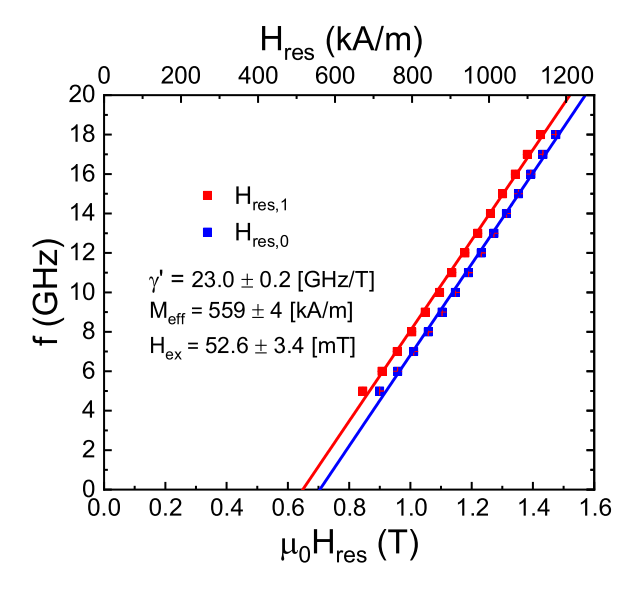


Fig. 4. Broadband out-of-plane FMR Kittel plots (resonant frequency as a function of \mathbf{H}_{res}).

Note that our dichroism experiments are only on the Fe sites, and we have no information on any contribution from Ge sites, which can carry some additional moment due to hybridization of states with Fe neighbors [35].

Based on the magnetic orbital to spin moment ratio, the spectroscopic splitting factor (g-factor, $g=2(1+\frac{m_l}{m_s}))$ [36,37] is estimated to be 2.3 ± 0.3 and 2.4 ± 0.3 for 72 nm and 18 nm thick films respectively. This calculated g-value is larger than 2.07 for cubic FeGe [38] and implies significant orbital contribution.

Dividing the total moment observed by SQUID magnetometry into approximate spin and orbital moment values based on the m_l/m_s ratios seen in XMCD, we arrive at spin moment contributions for both films matching the bulk all-spin moment value of 1 μ_B/f .u. The close agreement between the implied spin moment in our films and the ideal bulk value implies that the enhanced magnetization is due to strain-induced spin–orbit coupling and not due to measurement error. The results suggest a physical picture wherein a ~4% tensile strain does not significantly affect the spin configuration, spin moment, or the atomic ordering, but the decreased Fe–Fe bonding length increases the Curie temperature and generates spin–orbit coupling. Further, we cannot rule out strain-based effect as the source of spin–orbit coupling.

The magnetization dynamics in strained FeGe thin films were investigated by FMR spectroscopy using a broadband coplanar waveguide field-swept FMR setup at room temperature. Measurements were taken by applying a static magnetic field (H) both in IP and OP (to suppress two magnon scattering [39,40]) geometry (See Supplementary material for exemplary spectra, and IP measurement results [28]). Fig. 4 shows the Kittel plots for the 72 nm thick film. We observed two resonance fields $(H_{res,0})$ and $H_{res,1}$ at a given frequency (See Supplementary material [28] for exemplary spectra). The data sets were fitted together to find exchange field (H_{ex}) using the equation,

$$f(H_{res}) = \gamma'(H_{res} + H_{ex} - 4\pi M_{eff}), \tag{3}$$

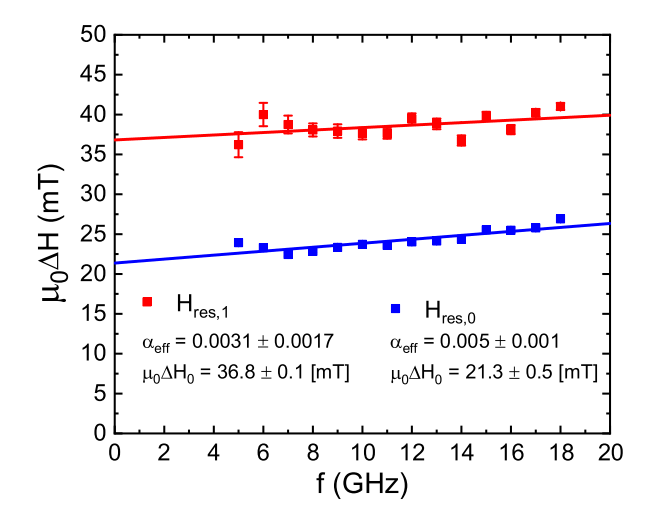


Fig. 5. Broadband out-of-plane FMR linewidths measured at room temperature for 72 nm FeGe film displaying a linear fit to determine the effective Gilbert damping parameter.

where, $H_{ex}=0$ for $H_{res,0}$ as this is the main resonance, γ' is the gyromagnetic ratio, and M_{eff} is the effective magnetization defined as $M_{eff}=M_s+\frac{2K_\perp}{4\pi M_s}$ (where K_\perp contains contributions from both a uniaxial perpendicular anisotropy and cubic anisotropy). The exchange field was found to be 52.6 ± 3.4 mT and by assuming perfect pinning of the spins at the surface can be used to calculate the exchange stiffness constant (A) using,

$$H_{res}(n=0) - H_{res}(n \neq 0) = H_{ex} = \frac{2A\pi^2 n^2}{M_s t_{FeGo}^2},$$
 (4)

where $M_s=186$ kA/m, n=0 is the main resonance and $n\neq 0$ is the perpendicular standing spin wave (PSSW) mode, and t is the film thickness for 72 nm thick film at room temperature [41,42]. The exchange stiffness constant was found to be 2.6×10^{-12} J/m which is smaller than reported by Porter et al. [43] and Ukleev et al. [34] for FeGe films. Fig. 5 shows that the extracted linewidth ΔH_{pp} scales linearly with the microwave frequency (f). This can be employed to determine the effective Gilbert damping parameter α_{eff} and quantify the FMR linewidth broadening contributions from magnetic inhomogeneities, using the equation [40,44],

$$\mu_0 \Delta H(f) = \mu_0 \Delta H_o + \frac{2}{\sqrt{3}} \frac{\alpha_{eff}}{\gamma'} f, \tag{5}$$

where ΔH_0 is the frequency-independent linewidth caused by inhomogeneity in the film. The inhomogeneous broadening (ΔH_0) for $H_{res,1}$ and $H_{res,0}$ were determined to be 36.8 \pm 0.1 mT (red curve) and 21.3 \pm 0.5 mT (blue curve) respectively. The effective damping parameter α_{eff} was found to be 0.0031 \pm 0.0017 for $H_{res,1}$ and 0.005 \pm 0.001 for $H_{res,0}$ respectively, much smaller than reported for bulk MnSi at 28 K [45] and FeGe film [46,47] grown on Si(111), but comparable to FeGe film [20] grown on MgO(100). The smaller value of the damping parameter is likely due to improved film quality. The observed value of effective Gilbert damping is smaller in the OP geometry suggesting significant two-magnon scattering contribution to magnetic relaxation in the in-plane geometry [39,40]. Low damping values are desirable for technological applications.

The values for gyromagnetic ratio (γ'), damping parameter, linewidth, and the effective magnetization M_{eff} at room temperature for 72 nm FeGe film are summarized in Table 2. From the calculated value for γ' in IP configuration, the calculated g-factor was found to be 2.27 for 72 nm in close agreement with that predicted by XMCD data. However, the gyromagnetic ratio γ' determined from the OP FMR data deviates significantly from both the IP data and the XMCD data.

Table 2Summary of gyromagnetic ratio, damping parameter, linewidth and effective magnetization for the 72 nm FeGe film in the out-of-plane (OP) and in-plane (IP) configuration.

Geometry	γ' [GHz/T]	$\begin{array}{c} \alpha_{eff} \\ [\times 10^{-3}] \end{array}$	$\mu_0 \Delta H_0$ [mT]	M _{eff} [kA/m]
OP	23.0 ± 0.2	3.1 ± 1.7* 5 ± 1**	36.8 ± 0.1* 21.3 ± 0.5**	559 ± 4
IP	31.8 ± 0.04	18.5 ± 0.5	20.3 ± 0.6	447 ± 3

Asterisks (*) and (**) refer to two resonant fields $H_{res,1}$ and $H_{res,0}$, respectively.

The maximum field of 1.6 T available in our FMR set up limited us to make measurements in the unsaturated regime for the perpendicular configuration which as was shown in [48] can lead to systematic errors in γ' and M_{eff} . In the perpendicular configuration this can lead to a systematically lower value for γ' and higher value for M_{eff} , consistent with our results.

In summary, we report evidence and careful characterization of substrate-induced strain enhancement of T_c to 350 K. We confirm a significant orbital moment not previously found in bulk or unstrained FeGe thin films, likely generated by tensile epitaxial strain. XA and XMCD demonstrate long-range magnetic ordering and suggest that the enhanced saturation magnetization as compared to bulk is likely due to spin–orbit coupling. Finally, a low effective Gilbert damping parameter by FMR spectroscopy, and g-factors of XMCD and FMR both corroborate significant orbital moment in the film.

See Supplementary material [28] for more information on XA, XMCD, and FMR.

S.B, K.M.L, and A.J.H. acknowledge support from the National Science Foundation (NSF), USA through NSF-CAREER Award No. DMR-2047251. Support is also acknowledged from the following National Science Foundation grants: NSF-CAREER Grant No. 1452670 (A.S.); DMR-1905662 (D.H); DMR-1904446 (M.E.J.). Support is acknowledged from the Air Force Office of Scientific Research, USA award FA9550-20-1-0247 (D.H.). Support is acknowledged from NASA, USA Grant NASA CAN80NSSC18M0023 (T.M.). This research used resources of the Advanced Light Source, a U.S. DOE Office of Science User Facility under contract no. DE-AC02-05CH11231. The authors gratefully acknowledge beamline scientists Padraic Shafer and Elke Arenholz at Beamline 4.0.2 at the Advanced Light Source, Lawrence Berkeley National Laboratory. The authors acknowledge Patrick Quarterman and Alexander J. Grutter for assistance in XA and XMCD measurements.

CRediT authorship contribution statement

Sujan Budhathoki: Conceptualization, Methodology, Data curation, Writing – original draft, Investigation. Arjun Sapkota: Investigation, Writing – review & editing, Data curation. Ka Ming Law: Investigation, Data curation. Smriti Ranjit: Investigation, Data curation. Gregory M. Stephen: Investigation, Data curation. Don Heiman: Supervision, Funding acquisition. Michelle E. Jamer: Supervision, Funding acquisition, Investigation, Data curation, Writing – review & editing. Tim Mewes: Supervision, Funding acquisition. Adam J. Hauser: Supervision, Conceptualization, Methodology, Funding acquisition, Investigation, Writing – review & editing, Project administration.

Declaration of competing interest

The authors declare that they have no known competing financial interests or personal relationships that could have appeared to influence the work reported in this paper.

Data availability

Data will be made available on request.

Appendix A. Supplementary data

Supplementary material related to this article can be found online at https://doi.org/10.1016/j.jmmm.2022.170053.

References

- [1] X. Yu, N. Kanazawa, Y. Onose, K. Kimoto, W. Zhang, S. Ishiwata, Y. Matsui, Y. Tokura, Nature Mater. 10 (2) (2011) 106.
- [2] N. Nagaosa, Y. Tokura, Nat. Nanotechnol. 8 (12) (2013) 899.
- [3] X. Yu, N. Kanazawa, W. Zhang, T. Nagai, T. Hara, K. Kimoto, Y. Matsui, Y. Onose, Y. Tokura, Nature Commun. 3 (2012) 988.
- [4] A. Fert, V. Cros, J. Sampaio, Nat. Nanotechnol. 8 (3) (2013) 152.
- [5] F. Jonietz, S. Mühlbauer, C. Pfleiderer, A. Neubauer, W. Münzer, A. Bauer, T. Adams, R. Georgii, P. Böni, R.A. Duine, et al., Science 330 (6011) (2010) 1648–1651.
- [6] I. Dzyaloshinsky, J. Phys. Chem. Solids 4 (4) (1958) 241-255.
- [7] T. Moriya, Phys. Rev. 120 (1960) 91–98.
- [8] A. Fert, N. Reyren, V. Cros, Nat. Rev. Mater. 2 (7) (2017) 17031.
- [9] S. Heinze, K. Von Bergmann, M. Menzel, J. Brede, A. Kubetzka, R. Wiesendanger, G. Bihlmayer, S. Blügel, Nat. Phys. 7 (9) (2011) 713.
- [10] N. Romming, C. Hanneken, M. Menzel, J.E. Bickel, B. Wolter, K. von Bergmann, A. Kubetzka, R. Wiesendanger, Science 341 (6146) (2013) 636–639.
- [11] G. Chen, T. Ma, A.T. N'Diaye, H. Kwon, C. Won, Y. Wu, A.K. Schmid, Nature Commun. 4 (2013) 2671.
- [12] C. Moreau-Luchaire, C. Moutafis, N. Reyren, J. Sampaio, C. Vaz, N. Van Horne, K. Bouzehouane, K. Garcia, C. Deranlot, P. Warnicke, et al., Nat. Nanotechnol. 11 (5) (2016) 444.
- [13] J. Gallagher, K. Meng, J. Brangham, H. Wang, B. Esser, D. McComb, F. Yang, Phys. Rev. Lett. 118 (2) (2017) 027201.
- [14] S. Mühlbauer, B. Binz, F. Jonietz, C. Pfleiderer, A. Rosch, A. Neubauer, R. Georgii, P. Böni, Science 323 (5916) (2009) 915–919.
- [15] X. Yu, Y. Onose, N. Kanazawa, J. Park, J. Han, Y. Matsui, N. Nagaosa, Y. Tokura, Nature 465 (7300) (2010) 901.
- [16] T. Adams, A. Chacon, M. Wagner, A. Bauer, G. Brandl, B. Pedersen, H. Berger, P. Lemmens, C. Pfleiderer, Phys. Rev. Lett. 108 (23) (2012) 237204.
- [17] W. Münzer, A. Neubauer, T. Adams, S. Mühlbauer, C. Franz, F. Jonietz, R. Georgii, P. Böni, B. Pedersen, M. Schmidt, et al., Phys. Rev. B 81 (4) (2010) 041203
- [18] S. Budhathoki, A. Sapkota, K.M. Law, S. Ranjit, B. Nepal, B.D. Hoskins, A.S. Thind, A.Y. Borisevich, M.E. Jamer, T.J. Anderson, et al., Phys. Rev. B 101 (22) (2020) 220405(R).
- [19] Y. Li, N. Kanazawa, X.Z. Yu, A. Tsukazaki, M. Kawasaki, M. Ichikawa, X.F. Jin, F. Kagawa, Y. Tokura, Phys. Rev. Lett. 110 (2013) 117202.
- [20] S. Zhang, I. Stasinopoulos, T. Lancaster, F. Xiao, A. Bauer, F. Rucker, A. Baker, A. Figueroa, Z. Salman, F. Pratt, et al., Sci. Rep. 7 (1) (2017) 123.
- [21] S. Budhathoki, A. Sapkota, K.M. Law, B. Nepal, S. Ranjit, K. Shambhu, T. Mewes, A.J. Hauser, J. Magn. Magn. Mater. 496 (2020) 165906.
- [22] K.M. Law, S. Budhathoki, S. Ranjit, F. Martin, A.S. Thind, R. Mishra, A.J. Hauser, Sci. Rep. 10 (1) (2020) 1–10.

- [23] P. Pedrazzini, H. Wilhelm, D. Jaccard, T. Jarlborg, M. Schmidt, M. Hanfland, L. Akselrud, H. Yuan, U. Schwarz, Y. Grin, et al., Phys. Rev. Lett. 98 (4) (2007) 047204.
- [24] H. Yamada, K. Terao, H. Ohta, E. Kulatov, Physica B: Condens. Matter 329 (2003) 1131–1133.
- [25] X. Zhang, Q. Lu, W. Liu, W. Niu, J. Sun, J. Cook, M. Vaninger, P.F. Miceli, D.J. Singh, S.-W. Lian, et al., Nature Commun. 12 (1) (2021) 1–9.
- [26] S.Y. Park, D.S. Kim, Y. Liu, J. Hwang, Y. Kim, W. Kim, J.-Y. Kim, C. Petrovic, C. Hwang, S.-K. Mo, et al., Nano Lett. 20 (1) (2019) 95–100.
- [27] A. Arrott, J.E. Noakes, Phys. Rev. Lett. 19 (14) (1967) 786.
- [28] Supplemental Material for "Ultralow Effective Gilbert Damping and Induced Orbital Moment in Strain-Engineered FeGe Films with Curie Temperature Exceeding Room Temperature" for Additional Information on XA, XMCD, and FMR Data.
- [29] J. Stöhr, H.C. Siegmann, Magnetism: From Fundamentals to Nanoscale Dynamics, Vol. 152, Springer Science & Business Media, 2007.
- [30] B. Thole, P. Carra, F. Sette, G. van der Laan, Phys. Rev. Lett. 68 (12) (1992)
- [31] P. Carra, B. Thole, M. Altarelli, X. Wang, Phys. Rev. Lett. 70 (5) (1993) 694.
- [32] C. Chen, Y. Idzerda, H. Lin, N. Smith, G. Meigs, E. Chaban, G. Ho, E. Pellegrin, F. Sette, Phys. Rev. Lett. 75 (1995) 152.
- [33] E. Goering, S. Gold, A. Bayer, Appl. Phys. A: Mater. Sci. Process. 78 (2004) 855.
- [34] V. Ukleev, O. Utesov, L. Yu, C. Luo, K. Chen, F. Radu, Y. Yamasaki, N. Kanazawa, Y. Tokura, T.-h. Arima, et al., Phys. Rev. Res. 3 (1) (2021) 013094.
- [35] F. Wilhelm, J. Sanchez, J.-P. Brison, D. Aoki, A. Shick, A. Rogalev, Phys. Rev. B. 95 (23) (2017) 235147.
- [36] J. Nibarger, R. Lopusnik, Z. Celinski, T. Silva, Appl. Phys. Lett. 83 (1) (2003) 93–95.
- [37] S. Chikazumi, C.D. Graham, Physics of Ferromagnetism 2e, (94) Oxford University Press on Demand, 2009.
- [38] S. Haraldson, L. Pettersson, S. Bhagat, J. Magn. Reson. (1969) 32 (1) (1978) 115–120.
- [39] K. Lenz, H. Wende, W. Kuch, K. Baberschke, K. Nagy, A. Jánossy, Phys. Rev. B 73 (14) (2006) 144424.
- [40] B. Heinrich, J. Cochran, R. Hasegawa, J. Appl. Phys. 57 (8) (1985) 3690-3692.
- [41] S. Klingler, A. Chumak, T. Mewes, B. Khodadadi, C. Mewes, C. Dubs, O. Surzhenko, B. Hillebrands, A. Conca, J. Phys. D: Appl. Phys. 48 (1) (2014) 015001.
- [42] F. Schreiber, Z. Frait, Phys. Rev. B 54 (9) (1996) 6473.
- [43] N.A. Porter, C.S. Spencer, R.C. Temple, C.J. Kinane, T.R. Charlton, S. Langridge, C.H. Marrows, Phys. Rev. B 92 (14) (2015) 144402.
- [44] R.D. McMichael, D. Twisselmann, A. Kunz, Phys. Rev. Lett. 90 (22) (2003) 227601.
- [45] T. Schwarze, J. Waizner, M. Garst, A. Bauer, I. Stasinopoulos, H. Berger, C. Pfleiderer, D. Grundler, Nature Mater. 14 (5) (2015) 478.
- [46] M. Beg, M. Albert, M.-A. Bisotti, D. Cortés-Ortuño, W. Wang, R. Carey, M. Vousden, O. Hovorka, C. Ciccarelli, C.S. Spencer, C.H. Marrows, H. Fangohr, Phys. Rev. B 95 (2017) 014433.
- [47] E. Turgut, A. Park, K. Nguyen, A. Moehle, D.A. Muller, G.D. Fuchs, Phys. Rev. B 95 (2017) 134416.
- [48] B. Khodadadi, J.B. Mohammadi, C. Mewes, T. Mewes, M. Manno, C. Leighton, C.W. Miller, Phys. Rev. B 96 (2017) 054436.